ADVANCED MATERIALS TECHNOLOGIES
www.advmattechnol.de

Facilitating Large-Scale Snow Shedding from In-Field Solar Arrays using Icephobic Surfaces with Low-Interfacial Toughness

*Abhishek Dhyani, Christopher Pike, Jennifer L. Braid, Erin Whitney, Laurie Burnham, and Anish Tuteja**

Large-scale accrual of snow and ice on solar arrays in northern latitudes can cause significant power generation losses during winter. Depending on environmental conditions, snow can encompass a wide range in physical characteristics from dry snow (modulus ≈100 kPa and density ≈0.1 g cm^{-3}) to bulk ice (modulus ≈8 GPa and density ≈0.9 g cm^{-3}). This variation in snow morphology has made the development of a passive, broad-spectrum, snow and ice-shedding surface challenging. Here, the authors develop one of the first surfaces that simultaneously possesses both low-interfacial strength ($\hat{\tau}_{ice}$ < 50 kPa) and toughness (Γ_{ice} < 0.5 J m^{-2}) with ice. These surfaces, fabricated via the addition of mobile polymer chains/oils to a thin polymeric coating, require extremely low detachment forces for ice, enabling its passive shedding at virtually any accretion length scale. Preliminary evidence that the new surfaces can shed different forms of snow and ice from field-deployed solar arrays, over a range of subzero temperatures for several weeks, leading to significant increases in power generation is provided. The optically transparent surfaces are easily scalable and can be widely deployed by the solar industry in areas that see persistent snow. Other applications include automotive windshields, LIDAR covers for autonomous vehicles, and cold climate optical sensors.

1. Introduction

The large-scale accretion of snow and ice on surfaces is a well-known risk to structural reliability, creating loads that can collapse roofs, compromise cold weather sensors, bring down power lines, and jeopardize the aerodynamics of airplane wings. More recently, there is growing recognition that photovoltaic (PV) systems in northern latitudes are also at risk from ice and snow loading.[1] Snow and ice-accretion on PV panels results in power generation losses as high as 80–100% relative to snow-free panels, and can—under extreme conditions—compromise the structural integrity of the panels by bending frames and cracking solar cells.[2,3] Considered across large PV systems and broad geographic areas, the drop in energy generation is significant, and may become even more concerning in view of changing weather patterns, which have resulted in record-breaking snow loads and cold temperatures across multiple latitudes; the polar vortex that swept Texas in 2021 being one such example.

Facilitating passive snow shedding from PV arrays is therefore of considerable interest to asset owners, investors, and underwriters. One challenge is that surfaces exposed to cold climates are prone to accrual of both snow and bulk ice, which adhere via different mechanisms to the underlying surface.[4,5] Another challenge is that snow can encompass a wide range of physical characteristics, such as structural morphology, phase composition, modulus (≈100 kPa to 8 GPa), density (0.1–0.9 g cm^{-3}), and accreted area, all of which vary with accumulation depth and ambient meteorological conditions.[6,7]

A. Dhyani, A. Tuteja
Macromolecular Science and Engineering
University of Michigan
2800 Plymouth Road, Ann Arbor, MI 48109, USA
E-mail: atuteja@umich.edu

A. Dhyani, A. Tuteja
BioInterfaces Institute
University of Michigan
2800 Plymouth Road, Ann Arbor, MI 48109, USA

C. Pike, E. Whitney
Alaska Center for Energy and Power
University of Alaska
1764 Tanana Loop, Fairbanks, AK 99775, USA

J. L. Braid, L. Burnham
Photovoltaics (PV) and Materials Technology Department
Sandia National Laboratories
Albuquerque, NM 87185, USA

A. Tuteja
Department of Materials Science and Engineering
University of Michigan
2800 Plymouth Road, Ann Arbor, MI 48109, USA

A. Tuteja
Department of Chemical Engineering
University of Michigan
2800 Plymouth Road, Ann Arbor, MI 48109, USA

The ORCID identification number(s) for the author(s) of this article can be found under https://doi.org/10.1002/admt.202101032.

DOI: 10.1002/admt.202101032

Therefore, a surface developed to reduce the accretion of a foulant such as snow, must consider multiple variables, including the foulant modulus and the foulant accreting length scales.[8–10] Icephobic coatings work well for shedding ice, but the extremely diverse physical characteristics of snow make the design of a single, broad spectrum de-icing surface difficult; and prior to this work, no scalable surface that consistently shows simultaneous snow and ice shedding, especially on a large scale (several m^2), has been demonstrated.

In this work, we develop optically transparent surfaces that possess both extremely low-interfacial strength ($\hat{\tau} < 50$ kPa) and low-interfacial toughness ($\Gamma < 0.5$ J m^{-2}). Such surfaces require low detachment forces and enable passive ice shedding over a wide range of accretion areas (from a few cm^2 up to 8 m^2). We also provide preliminary data to suggest this class of surfaces can consistently and repeatedly reduce the snow coverage on fielded solar arrays, and over a wide range of subzero temperatures (down to −35 °C), humidity, and wind conditions. Although our data are derived from a single test site in Alaska, where we applied each coating to a column of four PV modules, our data show that the coatings' ice- and snow-shedding performance is maintained over multiple months. Additionally, the passive snow shedding enabled by the developed coatings leads to a measurable and substantial increase in power generation (as high as 85%) from a single column of PV arrays.

The findings are substantial not only because of the coatings' potential to boost the efficiency of solar arrays in winter but also because their formulation represents a potentially new approach to passive snow removal. Most current approaches to enable the passive shedding of snow trace their development to surfaces that lower the adhesion of ice, i.e., icephobic surfaces.[11–13] Icephobic surfaces, or those surfaces that possess a lower interfacial strength (detachment force/area) with ice, $\hat{\tau}_{ice}$, can be developed by lowering the substrate surface energy,[14] minimizing contact area using texture,[15,16] lubrication,[17–19] interfacial cavitation,[20,21] or interfacial slippage.[22]

Although promising, icephobic surfaces suffer from one critical flaw: scalability. Because icephobic materials are characterized by low-interfacial strength, $\hat{\tau}_{ice}$, which is a shear *strength*, an increase in area necessitates a linear increase in the amount of applied force required to remove the ice. Thus, even surfaces possessing very low $\hat{\tau}_{ice}$ values require prohibitively high detachment forces to cause ice to shed from large, accreted areas (>few square meters), such as utility-scale solar arrays. Recently, a class of materials that exhibit a low interfacial toughness (LIT; $\Gamma < 1$ J m^{-2}) with ice has been developed.[23] LIT surfaces possess the unique property that the force required to remove any adhered ice is low, and independent of interfacial area because the delamination of ice (due to crack propagation at the interface between the ice and the coating) depends on the toughness of the interface and not its shear strength. As a result, the force required to de-bond a large interfacial area (few square meters) is the same as that required for a small area (few square centimeters) on LIT surfaces. Previous work has shown that the ice adhesion *strength* decreases as coating thickness increases and shear modulus decreases, while the ice interfacial *toughness* decreases as coating thickness decreases and shear modulus increases.[20,23] Thus, the material design requirements for icephobic and LIT surfaces are exactly the opposite of each other. As a result, it is hard to develop surfaces for which $\hat{\tau}_{ice} < 100$ kPa and $\Gamma < 1$ J m^{-2} simultaneously. This in turn implies that all the different ice shedding coatings developed thus far can facilitate the passive shedding of ice either for small (low $\hat{\tau}_{ice}$) or for large (low Γ) iced areas, but not both. Here, we discuss the development of coatings with $\hat{\tau}_{ice} < 50$ kPa and $\Gamma < 0.4$ J m^{-2}, allowing snow and ice shedding across broad length scales.

2. Fabrication and Testing of Coatings for Ice and Snow Shedding

2.1. Measurement of Interfacial Strength and Interfacial Toughness

In order to measure the interfacial strength and interfacial toughness of the ice-coating interface, we utilized a simple push-off setup, similar to that reported previously[23] (see the Experimental Section). Briefly, ice of different lengths (between 1 and 20 cm) was frozen onto each experimental surface adhered on a Peltier plate, set to a temperature of −10 °C. The force required to de-bond the ice ($\tilde{F}_{ice}$) was measured, and plotted against the length of ice, L, keeping the width and thickness constant (**Figure 1**a). There exists a critical bonded length of ice (L_c) below which the debonding between ice and the underlying substrate is dominated by interfacial strength ($\hat{\tau}$), and above which the debonding is controlled by interfacial toughness (Γ). L_c is given by

$$L_c = \sqrt{\frac{2E_{ice}\Gamma h}{\hat{\tau}_{ice}^2}} \tag{1}$$

where E_{ice} is the modulus of ice (≈8.5 GPa) of thickness h.[23] When bonded ice lengths (L) < L_c, interfacial strength dominates the fracture, and the force required to debond ice per unit width, $\tilde{F}_{ice}$, is proportional to L (Figure 1a). In this case, the ice adhesion strength can be computed as $\hat{\tau}_{ice} = \tilde{F}_{ice} / L$. When $L > L_c$, interfacial toughness dominates fracture, and the detachment force is constant for any interfacial length, $L > L_c$. This critical force, $\tilde{F}_{ice}^{cr}$, can be used to calculate Γ, using[24–26]

$$\Gamma = \frac{\left(\tilde{F}_{ice}^{cr}\right)^2}{2E_{ice}h} \tag{2}$$

Note that Γ and $\hat{\tau}$ values are likely to be different between snow and ice, due to the difference in the physical/mechanical properties between them.[4] For example, the modulus of snow can vary from ≈100 kPa to 8 GPa (that of bulk ice).

2.2. Controlling Interfacial Strength and Interfacial Toughness

A contributor to the coating-ice interfacial toughness is the deformation of the coating during the process of debonding. By using cohesive zone models, one can define the toughness of

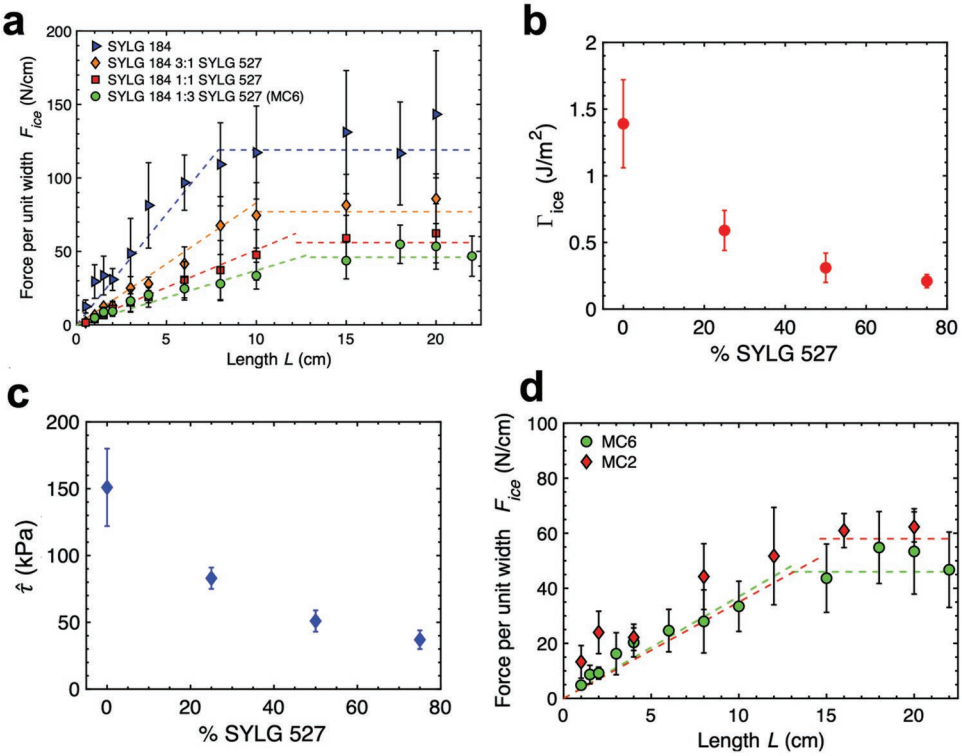

Figure 1. a) The force per unit width required to de-bond ice from thin silicone coatings ($t \sim 5$ µm each) with different amounts of SYLG 527. b) As the ratio of SYLG 527 to silicone content increases for four different coatings with $t \sim 5$ µm, Γ decreases. c) The effect of SYLG 527 content on $\hat{\tau}$ for four different silicone coatings with $t \sim 5$ µm also shows a decrease as its content increases. d) The force per unit width required to de-bond solid ice from the best-performing coatings MC2 (PVC + 60 wt% MCT, $t \sim 45$–50 µm) and MC6 (SYLG 184 1:3 SYLG 527, $t \sim 5$ µm). Both coatings had $\hat{\tau} < 50$ kPa and $\Gamma < 0.4$ J m^{-2}. All experimental results shown were obtained at –10 °C. Error bars represent one SD and $N \geq 5$.

an interface as the area under the force displacement curve of the entire interface, including the coating.[27,28] Assuming linear elasticity, the interfacial toughness for the coating–ice interface can be estimated as

$$\Gamma \approx \frac{\hat{\tau}^2 t}{2G} \tag{3}$$

where G is the shear modulus of the coating, and t is the thickness of the coating.[23] Therefore, lowering both the thickness and interfacial strength of the coating are essential to the development of snow/ice-shedding coatings.

Another essential criterion for the development of snow/ice-shedding coatings for PV modules is that the coatings be transparent (Figure S2, Supporting Information), and curable at temperatures as low as 0 °C to permit in-field application, if necessary. Further, these surfaces must repeatedly be able to shed snow and ice over a broad range of below-freezing operating temperatures, over long periods of time, and across widely different accreting length scales.

Surfaces that display low values of $\hat{\tau}_{ice}$ and Γ should be able to shed ice regardless of accretion length scales. To develop such coatings, we worked to modify commercially available rubbers and thermoplastics whose ice-shedding properties have been previously studied.[20,23] First, to systematically reduce $\hat{\tau}$ as well as Γ for ice, increasing quantities of an uncrosslinked, low-modulus prepolymer SYLG 527 (Sylgard 527) were blended with an uncrosslinked, high-modulus prepolymer SYLG 184 (Sylgard 184), and a crosslinker (see the Experimental Section). The blended coating was then applied to an aluminum substrate (with thickness $t \sim 5$ µm) and cured together. Note that this approach is different from previous work where holes were incorporated at predetermined locations within a higher modulus silicone to promote crack propagation via stiffness inhomogeneity.[29] This coating thickness is also orders of magnitude lower than state-of-the-art icephobic polymers,[20,29,30] and enables the reduction of the interfacial toughness of the fabricated coatings, as discussed above. Additionally, the low modulus and interfacial mobility of the polymer structure, i.e., silicone chains above their glass transition temperature, which are added as a crosslinker, produces low ice adhesion strength values for the fabricated coatings.[20,30–33]

Also of interest was the observation that increasing the proportion of the SYLG 527 from 0 to 75 wt% (MC6, see the Experimental Section), could reduce $\hat{\tau}$ from 151 ± 29 to 37 ± 7 kPa (Figure 1c). At the same time, Γ could be lowered from 1.39 ± 0.33 to 0.21 ± 0.05 J m^{-2} (Figure 1b). This formulation is the first known example of a surface that simultaneously displays extremely low-interfacial toughness ($\Gamma < 0.4$ J m^{-2}) and low-interfacial strength ($\hat{\tau} < 50$ kPa). In principle, such surfaces would require extremely low detachment forces for shedding accrued ice at both small and large accreting length scales. Note that the adhesion strength for dry snow can be three to four orders of magnitude lower than that of ice for the

same substrate over small accreted areas (few square centimeters),[4,14,23] and it is not clear from prior literature if a coating possessing low interfacial strength and toughness with ice would also be suitable for shedding different types of snow at different accreting length scales.

The approach of fabricating coatings that simultaneously display extremely low-interfacial toughness and low-interfacial strength by adding mobile polymer/oil chains to a thin polymeric coating is not limited to silicones. Previously, it has been shown that the addition of a plasticizer can lower the interfacial toughness of thermoplastics.[23] We similarly fabricated a surface with $\Gamma = 0.33 \pm 0.07$ J m^{-2} and $\hat{\tau} = 35 \pm 13$ kPa (Figure 1d) by incorporating 60 wt% of medium-chain triglyceride (MCT) oil to plasticize a common industrial polymer polyvinyl chloride (PVC), which is denoted as MC2 (Table S1, Supporting Information; see the Experimental Section). In this case, the coating thickness was higher, $t \sim 50$ µm, which increased the mechanical durability of the fabricated coating, as discussed below. Note, MC2 has a higher MCT content and more than an order of magnitude higher thickness than the system reported in our previous work.[23]

3. In-Field Snow-Shedding Performance

3.1. Changing Physical Properties of Snow

Different ambient conditions can lead to different structural forms of snow and ice.[6] For example, dense and sticky wet snow with high moisture content can form when air temperatures (T_{air}) are above −3 °C, i.e., a few degrees below the freezing point, whereas dry, powdery snow forms below this temperature.[4,16,34] Snow can also metamorphose (undergo structural changes that increase its density) as a result of thermodynamic processes, packing and/or deformation under its own weight.[6] Indeed, under its own weight, snow can increase in density to the point that its cohesive strength becomes higher than the shear strength of the snow–substrate interface,[35] resulting in displacement and possible debonding at the interface before cohesive failure. Additionally, snow sintering to form bulk ice can occur at temperatures between −10 and 0° C.[6] Wet snow, either from snowfall or melting, can also re-freeze to form layers of solid ice.[4] This mutability underscores the need for coatings for PV applications that have both snow-phobic and icephobic properties, as well as the need for field demonstrations that capture a full range of ambient conditions in winter.

3.2. Field Demonstration

To evaluate their performance under realistic wintry conditions, the MC6 and MC2 formulations were shipped to the University of Alaska, Fairbanks, for application to a subset of 72 cell (2 m × 1 m) PV modules at a utility-owned, grid-tied PV site in Fairbanks, Alaska (Lat 64.8°), for the winter of 2019–2020. The tilt angle of the installed PV arrays, which can influence snow sliding, was maintained at 45°.

Sixteen modules were removed from the arrays and the coatings were applied indoors at room temperature, sorted into two experimental cohorts: 1) MC6 applied to the module surface glass and structural frame; and 2) MC2 applied to the module surface glass and structural frame. At the test site, the modules are mounted four-up in landscape orientation, and connected via microinverters. Each column of coated modules is separated by a column of uncoated modules to avoid any unintended interference by an adjacent coated column. Data on snow shedding were collected by a research-grade camera positioned normal to each array and with a field-of-view sufficient to capture the full array of experimental panels. The cameras were programmed to take images every 15 min during daylight hours, with data transmitted for analysis (see the Experimental Section). Synchronized, time-stamped weather data were also collected.

3.3. Results and Analysis

In our analysis of the collected field data, we consider a reduction in snow coverage by 20% over 15 min (consequent images) as a major snow shedding event, although smaller shedding events were also observed to occur over time (**Figure 2**). In one instance, a light, dry snowfall at T_{air} between −10 and −15 °C and low absolute humidity (<2 g m^{-3}) deposited a thin snow layer (thickness less than 2 mm) on the modules overnight. In a matter of minutes, both the MC2 and MC6 columns showed accelerated snow shedding, relative to the uncoated control column, with snow coverage reduced by ≈61% and ≈32% on MC2 and MC6, respectively (Figure 2a–d). The uncoated modules, on the other hand, remained completely covered with snow (≈95–100%) for >2 weeks, missing power generation opportunities. The MC2-coated panel showed similar shedding events over repeated snowfall during the coming weeks (Figure 2a–d). While wind can be a contributing factor to snow loss from a surface, the wind speed recorded on site during this shedding event was negligible (<0.1 m s^{-1}), indicating that the snow shed passively under the inertia of its own weight. These results are significant because the ability to shed thin sheets of dry snow, which is the least dense form of snow and therefore hardest to shed, highlights the fact that combined low-interfacial toughness and low-interfacial strength surfaces can precipitate the shedding of most types of snow.

Additional data were collected from the Fairbanks site under conditions where T_{air} was close to −3 °C and absolute humidity (ρ_v) was measured at ≈3 g m^{-3} (characteristics of wet snow), between February 8 and February 9. In just a few hours after snowfall, the sheets of wet snow shed from a light gust of wind at speeds of just 0.5 m s^{-1}, reducing the snow coverage area by ≈86% on the MC2-coated column (Figure 2e–g). This observation again highlights the extremely low shear forces needed to detach thin sheets of snow. Data collected over a 2 week time frame, show the MC2-coated column removed snow coverage repeatedly over three snowfall events, whereas the uncoated modules remained covered in snow (100%) for over 2 weeks. These results represent the benefit of a snow-free panel and the difference it can cause in solar resource availability and power generation (Figure 2e).

The Fairbanks site also provided data on the coatings' performance against metamorphosed snow. On February 6, fresh snow fell at $T_{air} \sim -3$ °C and remained undisturbed for more

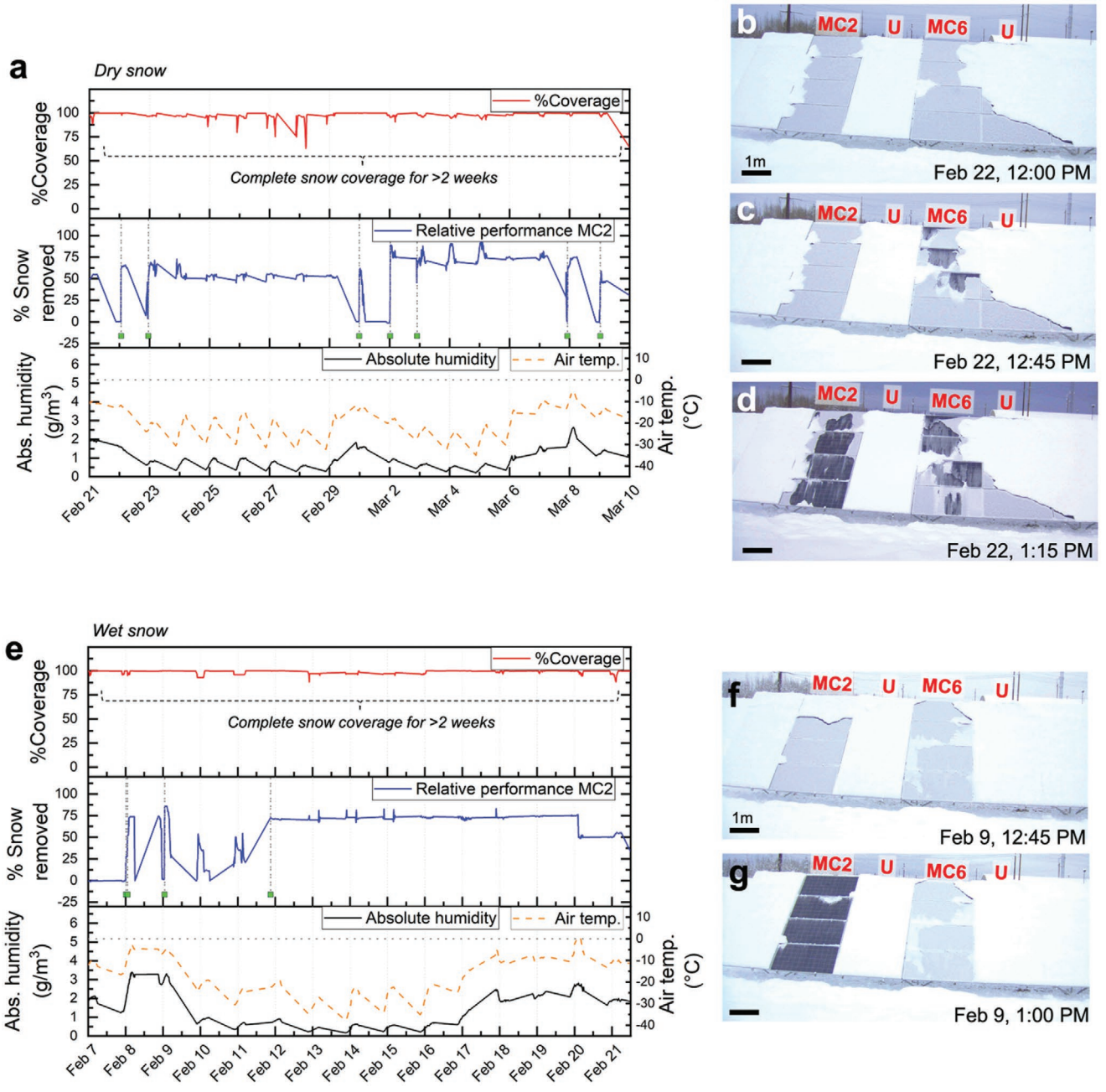

Figure 2. a) Comparison of snow coverage during periods of *dry snowfall* on an uncoated module (U), modules coated with MC2 and MC6, over a range of T_{air} between –6 and –35 °C in the Fairbanks site during February–March 2020. Green drop points highlight major snow shedding events as defined in the text. b–d) Images from specific timestamps show thin sheets (thickness < 2 mm) of dry snow coverage and shedding corresponding to data shown in (a). e) Comparison of *wet snow coverage* on uncoated and MC2 coated columns. Wet snow settled between February 8 and February 9, and icy snow was formed from February 9 to February 12. Both types of snow were shed from MC2. Green drop points represent major snow shedding events. f,g) MC2-coated column right before the onset of wet snow shedding at T_{air} ~ –3 °C and absolute humidity ≈3 g m^{-3}. In just a few hours after snowfall, the sheets of wet snow shed from a light gust of wind at speeds of just 0.5 m s^{-1}, reducing the snow coverage area by ≈86% on the MC2-coated column. This observation highlights the extremely low shear forces needed to blow off thin sheets of snow.

than 50 h on all panels at a wide air temperature range between –6 and –16 °C. The MC6-coated column shed ≈40–50% of its snow cover just 12 h after snowfall, when the ambient air temperature ranged from –7 to –13 °C (**Figure 3**a–d). In contrast, the MC2-coated modules retained their snow cover for 50 h, during which time the snow metamorphosed leading to a more rigid microstructure and snow with much higher density.[6] After this period, large 2 m × 1 m sections (≈30 mm thickness) of the dense, hard snow sheet detached from the MC2 interface, exposing a full 75% of the column area to sunlight (Figure 3a,e–g). The difference in performance is likely attributable to the lower interfacial toughness of MC6

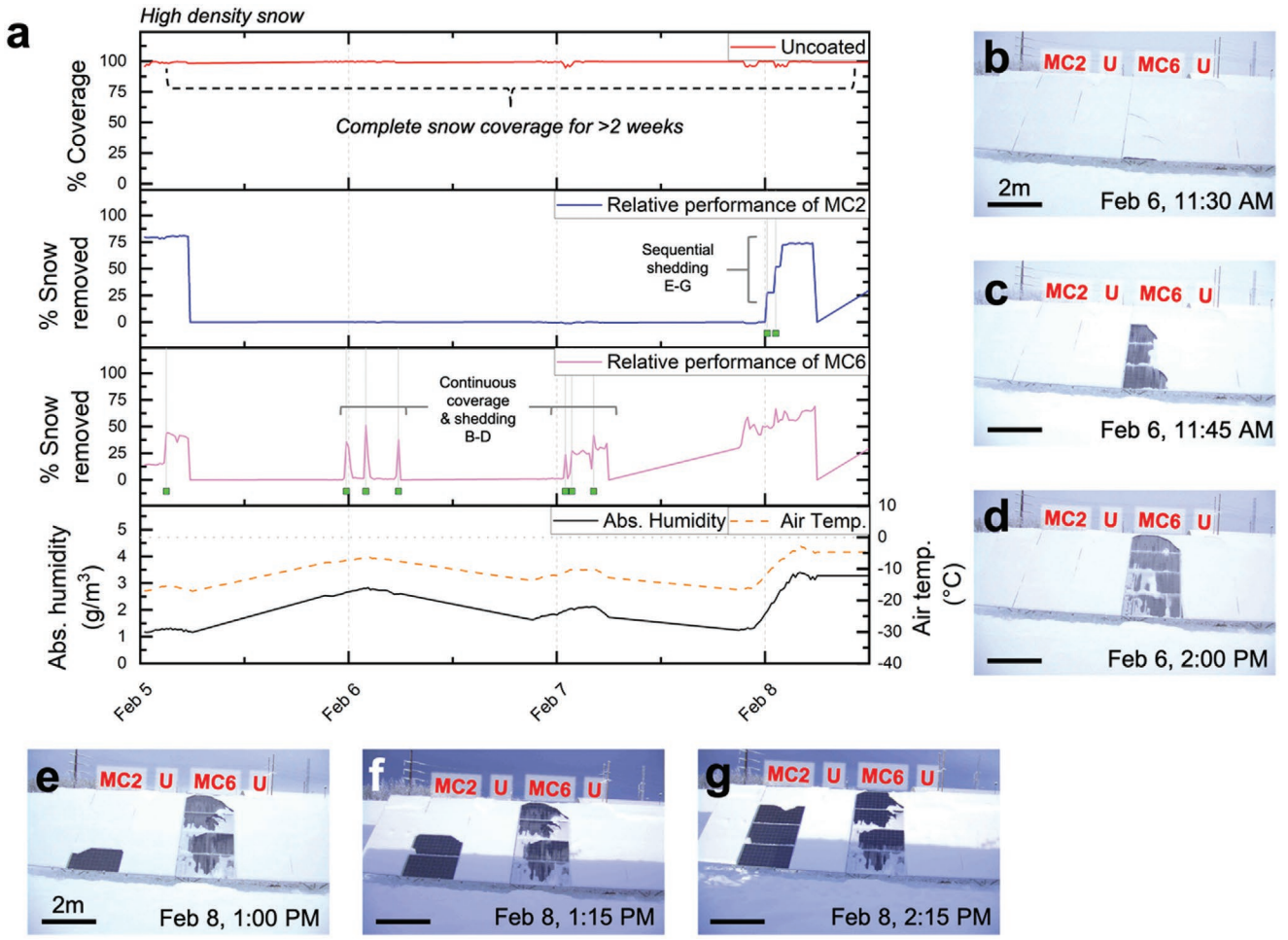

Figure 3. a) Comparison of high density (crusty/hard) snow coverage on an uncoated module (U), modules coated with MC2 and MC6, and only module frames coated with MC2 (MC2F) and MC6 (MC6F) with absolute humidity and T_{air} in February 2020 (Fairbanks). Green drop points highlight major snow shedding events as defined previously. b–g) Images from specific timestamps showing ice and snow coverage and shedding corresponding to data shown in (a).

($\Gamma = 0.21 \pm 0.05$ J m^{-2}, $\tilde{F}_{ice}^{cr} = 46 \pm 6$ N cm^{-1}) as compared to that for MC2 ($\Gamma = 0.33 \pm 0.07$ J m^{-2}, $\tilde{F}_{ice}^{cr} = 58 \pm 7$ N cm^{-1}). In another instance from February 9 to February 12, fresh snow, which settled at $T_{air} \sim -3$ °C, experienced significant temperature fluctuations (from ≈ −3 to −31 °C to −20 °C) over the course of 66 h (Figure 2e–g). At the end of the 66 h, 70% of snow on the MC2-coated column had shed, leaving 30% of residual snow, whereas the control column had retained 100% of their snow cover for over 2 weeks. In our observation, dry snow (higher porosity) required lower thicknesses (and therefore weight) to shed, while more rigid snow (frozen from wet snow) required a larger thickness to shed.

These findings provide preliminary evidence that surfaces possessing low-interfacial toughness and low-interfacial strength with ice can be useful for passively shedding different forms of snow in situ over wide subzero temperature and humidity ranges. The findings also show that MC2 performed on average better than either MC6 or the uncoated control (**Figure 4**). The performance differences are documented by snow coverage data: the MC2-coated panels had an average snow coverage amount of 27.7%, whereas the MC6 panels, had an average snow coverage of 45.4% (Figure 4b). The monthly snow coverage data in Figure 4a shows the extremely low average snow accumulation on the MC2 (≈32%) and MC6 (≈55%)-coated modules in comparison to >80% areal snow coverage on both uncoated modules U1 and U2. This indicates significant differences between uncoated and coated solar arrays during periods of heavy snowfall and improved opportunities for energy generation within such weather/climate conditions. The higher average snow coverage of the MC6 coating relative to MC2 is better understood by Figure 4a, where MC6 exhibits a degradation in performance over the course of the winter. This can be attributed likely to its lower mechanical strength, which resulted in delamination from the module glass, and the exposure of uncoated areas of the module surface that increased snow adhesion over time. In contrast, MC2 maintained its performance over the entire 77 day experiment. The fact that multiple shedding events occurred consistently throughout the winter, also highlights the MC2 coating's durability.

The above results are most interesting from a power-generation perspective because utility utility-scale PV system power loss and photovoltaic energy yield on both coated and uncoated

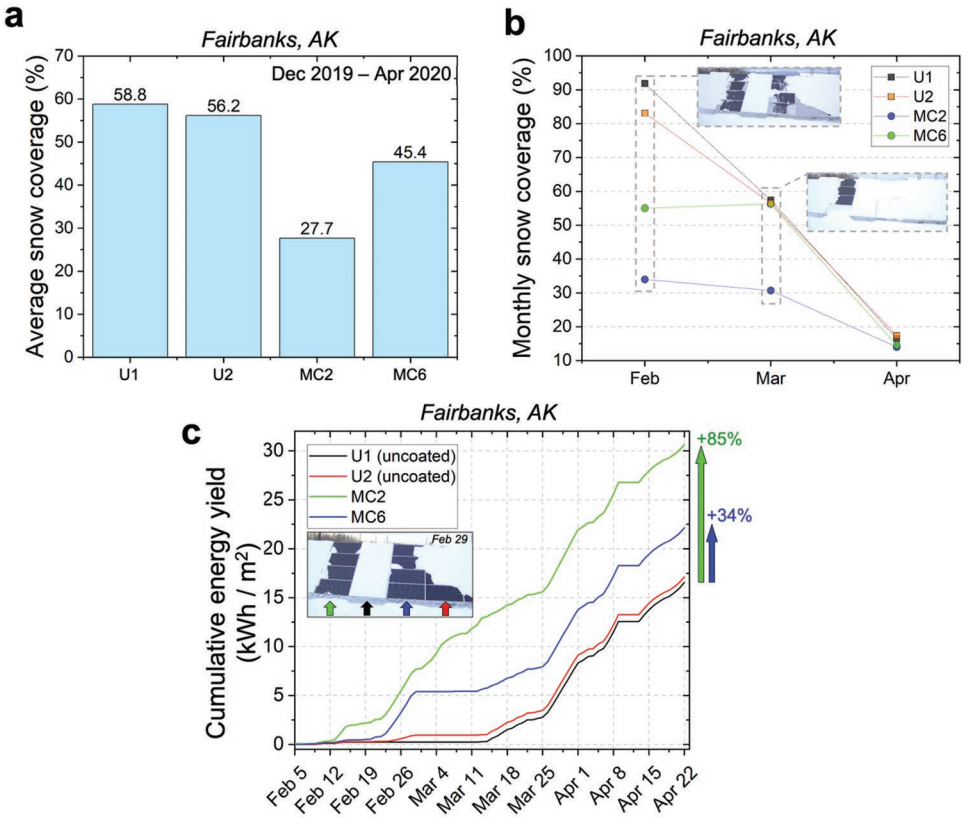

Figure 4. a) Monthly snow coverage on different uncoated (U1 and U2) and coated (MC2 and MC6) module surfaces over 3 months in Fairbanks. Insets show timestamp images for light and heavy snow loads of thin (≈2 mm) and thick (>300 mm) snow sheets shedding during respective months over the coated modules (see Figures 2 and 3 for module labels). b) Average snow coverage on different module surfaces over the entire 77 day testing period in Fairbanks. Insets show optical images of the panels after shedding events in February and March. c) Cumulative energy yield (kWh m^{-2}) from an average of three analytical methods for different uncoated (U1 and U2) and coated (MC2 and MC6) modules over 77 days. The energy yield corresponds to a bare panel efficiency of 16% and would likely be higher for more efficient panels. Inset shows a timestamp with snow-free coated panels corresponding to an energy yield increase.

panels was estimated using three distinct methods (see the Experimental Section). The rapid shedding of snow from the surface of a single MC2-coated column resulted in a cumulative increase in energy yield per module of ≈79–85%, relative to the uncoated columns after the end of winter (Figure 4c, **Table 1**). Meanwhile, the MC6-coated column resulted in a cumulative increase in energy yield of ≈29–34%, relative to the uncoated columns (Figure 4c, Table 1). These improvements in energy production over a single column of coated PV arrays become extremely significant when considered across large areas and broad geographic regions over multiple latitudes.

Table 1. Estimated energy yield per module for uncoated (U1 and U2) and coated (MC2 and MC6) modules in this study over 77 days calculated using three different methods. The increase in energy is fairly consistent among the three methods employed for DC power loss estimation and shows an ≈79–85% increase in energy yield for a single MC2 column relative to the uncoated columns and an ≈29–34% increase for a single MC6 column.

Analysis method	Estimated energy yield per module [kWh] over 77 days			
	U1	U2	MC2	MC6
Image	34.8	36.6	60	43.7
PVLIB	35.3	37.3	64	47.5
2X	29.3	28.9	59.9	41.8
Average	33.1	34.3	61.3 (+79–85%)	44.3 (+29–34%)

4. Conclusions

The development of a single, effective strategy to accelerate the detachment and shedding of snow and ice from a surface has historically proved problematic. By adding mobile polymer chains/oils to a thin polymeric coating, we fabricate one of the first coating systems that simultaneously displays low-interfacial strength and low-interfacial toughness with ice. Such surfaces can facilitate ice shedding across virtually any accreted length scale. In a preliminary demonstration during the winter of 2019–2020, the developed coatings enabled the repeated, passive shedding of snow and ice from in-field solar arrays in sub-arctic, winter conditions over several weeks, thereby significantly increasing the energy yield for coated PV modules (up to 85% more). While further validation studies are needed at multiple northern locations, including the analysis of power gains for different climate profiles and longitudinal studies to determine the coatings' long-term efficacy and durability, the

findings presented here have major implications for increasing the productivity and availability of solar energy systems in cold climates. Moreover, this new class of ice and snow-shedding coatings is expected to have multiple applications, where optical transparency is paramount, including building-integrated PV, as well as LiDAR, car windshields, optical sensors, etc., that are mission critical, but vulnerable to snow and ice adhesion in winter.

5. Experimental Section

Coating Fabrication and Application: Sylgard 184 (Dow Silicones) was fabricated in a 10:1 base:crosslinker ratio, while Sylgard 527 (Dow Silicones) was fabricated in a 1:1 base:crosslinker ratio, per manufacturer instructions. To achieve different ratios of Sylgard 184 and Sylgard 527, the precursors were mixed accordingly and dissolved in hexane (50 mg mL^{-1}). The mixture was vortexed until homogenous, degassed to remove bubbles, and brushed onto the Al substrates for ice adhesion testing and glass substrates for optical transparency measurements. The samples were then cured at 150 °C for 1 h. The samples may also be cured at room temperature. For cold temperature curing for outdoor application, DOWSIL 3-6559 (Dow Inc.) may be added (see below). All the coatings exhibited a similar ratio of advancing contact angle to receding contact angle of $\theta_{adv}/\theta_{rec} = 113°/101°$.

To fabricate plasticized PVC coatings, polyvinyl chloride ($M_w = 120\,000$, Scientific Polymer) was dissolved in tetrahydrofuran (THF) at a 100 mg mL^{-1} ratio. Once fully dissolved, medium-chain triglyceride oil (MCT, Jedwards International) was added to the solution at 60 wt%, to generate a plasticized coating. The systems were homogenized using a vortexer at room temperature. After homogenization, the solutions were brush coated onto aluminum substrates and left to dry for 24 h. This resulted in a coating with thickness ≈50 µm (as measured using a Mitotoyo micrometer), depending on the initial concentration. All the coatings exhibited a similar ratio of advancing contact angle to receding contact angle of $\theta_{adv}/\theta_{rec} = 92°/80°$.

To apply MC2 to the PV module, a 100 mg mL^{-1} solution of PVC + 60 wt% MCT oil in THF solvent was made. THF dissolved most plastics so it was essential to use a glass container for dissolution. For brush coat application over a 150 ft^2 panel, 150 g of PVC powder and 225 g of MCT oil were mixed. ≈3.75 L of THF was used to dissolve the above mixture in a glass container. A paint mixer attached to a drill was used as the stirring apparatus to make sure the solution was homogenously mixed. The container was sealed during stirring and used to avoid evaporation of the solvent. PV modules were removed from the arrays and brought indoors and allowed to warm to ≈15 °C. Any moisture present on the modules was removed. The modules were positioned horizontally and the coatings were applied in a single layer with a 7.6 cm paint brush commonly used to apply paint and varnishes to furniture. The coatings were allowed to cure for ≈24 h and the PV modules were reinstalled at the arrays. A flat or fan brush was used for brush coating. The solution was applied over the substrate panel in a single stroke. Only one layer of coating was applied to avoid surface irregularities. The coating was left to dry for 24 h.

To fabricate MC6 for the large PV modules, a 50 mg mL^{-1} solution of 20 wt% DOWSIL 3-6559 Accelerator, 20 wt% Sylgard 184, and 60 wt% Sylgard 527 in hexane solvent (50 mg mL^{-1}) was made. 20 wt% DOWSIL 3-6559 was added to the mixture to facilitate curing at low temperatures. Hexane does not dissolve HDPE or PP containers and they were used for dissolution. Glass containers were also be used. For brush coat application over a 150 ft^2 panel, 65 g of Sylgard 184 part A, 107.5 g of Sylgard 527 part A, and 71.5 g of DOWSIL 3-6559 accelerator were weighed. ≈7.2 L of hexane was used to dissolve the above mixture in a glass, HDPE, or PP container. A paint mixer attached to a drill was used as the stirring apparatus to make sure the solution was homogenously mixed. The container was sealed during stirring to avoid evaporation of the solvent. Once the mixture was fully dissolved, 6.5 g of Sylgard 184 part B and 107.5 g of Sylgard 527 part B were added to the above mixture and mixed thoroughly. Once the cure agents were mixed in, ≈40 min of working time was available before the coating cured at room temperature. If the coating was mixed/applied in a colder environment (4 °C), the working time was 1–2 h. A flat or fan brush was used for brush coating. The solution was applied over the substrate panel in a single stroke. The container was sealed after use to avoid solvent evaporation. The coating was cured overnight at room temperature. If the cure temperature was 4 °C, 2 days were used to cure.

Optical Transparency Measurements: UV absorption data were collected on a Varian Cary 50 Bio spectrometer. The scanning range was 300–800 nm.

Ice Adhesion Measurements: The measurements of τ_{ice} and $\tilde{F}_{ice}$ were conducted in a similar fashion to techniques reported previously.[23] To observe a critical length during ice-adhesion testing, a Peltier-plate system was used. The Peltier-plate system used in this work (Laird Technologies) measured 22 cm in length and 6 cm in width (Figure S1, Supporting Information). The sample to be tested was prepared to fit this geometry and adhered to the plate using double-sided tape (3M Company). To evaluate different lengths of interfacial area in a relatively short amount of time, and to maximize consistency between tests, the entire substrate was used for ice-adhesion testing. For example, in Figure S1 a typical test is shown, where 11 different pieces of ice were all frozen together. Short- and long-length samples were placed within the geometry of the Peltier plate at random locations on the surface to confirm that the measurements did not affect one another. In all these experiments, lengths from 0.5 to 20 cm were used. In total, a minimum of five measurements ($N = 5$) were taken for each length. The height and width of ice were fixed at $h = 0.6$ cm and $w = 1$ cm. The ice was frozen at –10 °C. The force required to dislodge the ice was recorded using a force gauge (Nextech DFS500) at a controlled velocity of 74 µm s^{-1} (Figure S1).

Weather Data, Image Acquisition, and Analysis: An identical weather station and camera were used at both locations to collect images as well as plan of array (POA) irradiance, temperature, relative humidity, wind speed, and wind direction. A CCFC Campbell Scientific field camera was used to record images at a 15 min interval during daylight hours. Images were analyzed using ImageJ software. Irradiance was measured with a Campbell Scientific CS320 pyranometer. The CS320 is an ISO 9060 second class instrument with an internal heater to minimize liquid and frozen contamination. Temperature and relative humidity were measured with a Campbell Scientific HygroVUE10 sensor located in a solar radiation shield. Wind speed and direction were measured with a RM Young 3002 cup style anemometer. It had a velocity accuracy of ±0.5 m s^{-1} and directional accuracy of ±5°. All weather data were measured at 5 s intervals and averaged to 1 min intervals using a Campbell Scientific CR1000X data logger.

Modeling Energy Yield: Power loss was estimated for each test group (column) of modules in three ways: 1) the pvlib implementation of the NREL method for estimating DC power loss based on percentage of snow coverage;[36] 2) assuming twice the power loss as the percentage of snow coverage;[37] and 3) a spatial-electrical model developed in previous work.[38] The latter considered the physical distribution of snow on each cell string (and each cell in that string), estimated the local maximum power points of the module- or string-level *I–V* curve for the system based on bypass diode behavior for each cell string, and selected the global maximum power point for power loss calculation. For each of the three methods employed, each column of like-coated modules was considered as a system of four modules connected in series, with three cell strings in each module. The resulting 15 min power loss estimations were applied to the modeled time-series power for an unshaded system. Power was modeled for a single 320 W panel at Fairbanks site using the PV Watts performance model for each 15 min period.[39]

Statistical Analysis: The interfacial shear strength, $\hat{\tau}$, was taken from the slope of the $\tilde{F}_{ice}$ against L fit in the linear (strength-controlled) regime. For consistency, lengths were included in the linear fit that minimized the overall error in the measurement of $\hat{\tau}$.

For each length of ice, several measurements were taken. For each reported value of $\tilde{F}_{ice}$, the data point was the mean of at least five

measurements, $\tilde{F}_L$, and the error bar was one standard deviation, Ω_{ice}. The error in $\hat{\tau}$, equivalently the error in the slope, was found using

$$\Omega_\tau = \sqrt{\frac{1}{\Delta}\sum\frac{1}{\Omega_L^2}} \tag{4}$$

where Δ was given by

$$\Delta = \sum\frac{1}{\Omega_L^2}\sum\frac{\tilde{F}_L^2}{\Omega_L^2} - \left(\sum\frac{\tilde{F}_L}{\Omega_L}\right)^2 \tag{5}$$

Once the best fit for $\hat{\tau}$ was found using the method described above, $\tilde{F}_{ice}^{cr}$ was determined by averaging the recorded $\tilde{F}_{ice}$ values for all $L > L_c$. The error in the intercept of the best-fit line for $\hat{\tau}$, Ω_{τ_b}, was found using

$$\Omega_{\tau_b} = \sqrt{\frac{1}{\Delta}\sum\frac{\tilde{F}_L^2}{\Omega_L^2}} \tag{6}$$

The critical interfacial length, L_c, was found from the intersection of the linear fit in the strength-controlled regime ($\hat{\tau}$) and the mean value of $\tilde{F}_{ice}^{cr}$ in the toughness-controlled regime.

Supporting Information

Supporting Information is available from the Wiley Online Library or from the author.

Acknowledgements

This work was funded in part or whole by the U.S. Department of Energy Solar Energy Technologies Office, under Award Number 34363.

Conflict of Interest

The authors declare no conflict of interest.

Author Contributions

All authors designed the experiments, wrote, and/or edited the manuscript. A.D. formulated and tested the surfaces for ice adhesion experiments. C.P. and E.W. fabricated the coatings formulated by A.D. and coated the solar arrays. A.D., C.P., and J.L.B conducted the image analysis for snow shedding and power generation performance. E.W., L.B., and A.T. conceived the research.

Data Availability Statement

The data that support the findings of this study are available from the corresponding author upon reasonable request.

Keywords

coatings, icephobic, interfacial toughness, photovoltaics, snow shedding

Received: August 15, 2021
Revised: October 18, 2021
Published online: November 23, 2021

[1] E. Andenæs, B. P. Jelle, K. Ramlo, T. Kolås, J. Selj, S. E. Foss, *Sol. Energy* **2018**, *159*, 318.
[2] L. Powers, J. Newmiller, T. Townsend, in *2010 35th IEEE Photovoltaic Specialists Conf*, IEEE, Piscataway, NJ **2010**, pp. 000973–000978.
[3] R. E. Pawluk, Y. Chen, Y. She, *Renewable Sustainable Energy Rev.* **2019**, *107*, 171.
[4] J. Heil, B. Mohammadian, M. Sarayloo, K. Bruns, H. Sojoudi, *Appl. Sci.* **2020**, *10*, 5407.
[5] P.-O. A. Borrebæk, B. P. Jelle, Z. Zhang, *Sol. Energy Mater. Sol. Cells* **2020**, *206*, 110306.
[6] J. R. Blackford, *J. Phys. D: Appl. Phys.* **2007**, *40*, R355.
[7] L. Makkonen, *Philos. Trans. R. Soc. London, Ser. A* **2000**, *358*, 2913.
[8] A. K. Halvey, B. Macdonald, A. Dhyani, A. Tuteja, *Philos. Trans. R. Soc., A* **2019**, *377*, 20180266.
[9] J. Y. Chung, M. K. Chaudhury, *J. Adhes.* **2005**, *81*, 1119.
[10] A. Dhyani, J. Wang, A. K. Halvey, B. Macdonald, G. Mehta, A. Tuteja, *Science* **2021**, *373*, eaba5010.
[11] L. B. Boinovich, A. M. Emelyanenko, K. A. Emelyanenko, E. B. Modin, *ACS Nano* **2019**, *13*, 4335.
[12] L. B. Boinovich, A. M. Emelyanenko, V. K. Ivanov, A. S. Pashinin, *ACS Appl. Mater. Interfaces* **2013**, *5*, 2549.
[13] M. Balordi, A. Cammi, C. Chemelli, P. Marcacci, G. Pirovano, G. Santucci, in *IWAIS*, **2019**.
[14] A. J. Meuler, J. D. Smith, K. K. Varanasi, J. M. Mabry, G. H. McKinley, R. E. Cohen, *ACS Appl. Mater. Interfaces* **2010**, *2*, 3100.
[15] S. Kulinich, M. Farzaneh, *Appl. Surf. Sci.* **2009**, *255*, 8153.
[16] H. Sojoudi, M. Wang, N. Boscher, G. H. McKinley, K. K. Gleason, *Soft Matter* **2016**, *12*, 1938.
[17] P. Kim, T.-S. Wong, J. Alvarenga, M. J. Kreder, W. E. Adorno-Martinez, J. Aizenberg, *ACS Nano* **2012**, *6*, 6569.
[18] R. Dou, J. Chen, Y. Zhang, X. Wang, D. Cui, Y. Song, L. Jiang, J. Wang, *ACS Appl. Mater. Interfaces* **2014**, *6*, 6998.
[19] Y. H. Yeong, A. Milionis, E. Loth, J. Sokhey, *Cold Reg. Sci. Technol.* **2018**, *148*, 29.
[20] K. Golovin, S. P. Kobaku, D. H. Lee, E. T. DiLoreto, J. M. Mabry, A. Tuteja, *Sci. Adv.* **2016**, *2*, e1501496.
[21] D. L. Beemer, W. Wang, A. K. Kota, *J. Mater. Chem. A* **2016**, *4*, 18253.
[22] K. Golovin, A. Tuteja, *Sci. Adv.* **2017**, *3*, e1701617.
[23] K. Golovin, A. Dhyani, M. D. Thouless, A. Tuteja, *Science* **2019**, *364*, 371.
[24] Z. Suo, J. W. Hutchinson, *Int. J. Fract.* **1990**, *43*, 1.
[25] M. Thouless, A. Evans, M. Ashby, J. Hutchinson, *Acta Metall.* **1987**, *35*, 1333.
[26] M. D. Thouless, *J. Vac. Sci. Technol., A* **1991**, *9*, 2510.
[27] R. Sills, M. Thouless, *Int. J. Solids Struct.* **2015**, *55*, 32.
[28] R. Sills, M. Thouless, *Eng. Fract. Mech.* **2013**, *109*, 353.
[29] Z. He, S. Xiao, H. Gao, J. He, Z. Zhang, *Soft Matter* **2017**, *13*, 6562.
[30] P. Irajizad, A. Al-Bayati, B. Eslami, T. Shafquat, M. Nazari, P. Jafari, V. Kashyap, A. Masoudi, D. Araya, H. Ghasemi, *Mater. Horiz.* **2019**, *6*, 758.
[31] L. Zhang, Z. Guo, J. Sarma, X. Dai, *ACS Appl. Mater. Interfaces* **2020**, *12*, 20084.
[32] Z. He, Y. Zhuo, J. He, Z. Zhang, *Soft Matter* **2018**, *14*, 4846.
[33] L. Zhu, J. Xue, Y. Wang, Q. Chen, J. Ding, Q. Wang, *ACS Appl. Mater. Interfaces* **2013**, *5*, 4053.
[34] R. Pfister, M. Schneebeli, *Hydrol. Processes* **1999**, *13*, 2345.
[35] M. Mellor, *A Review of Basic Snow Mechanics*, US Army Cold Regions Research and Engineering Laboratory, Hanover, NH **1974**.
[36] P. Gilman, N. A. DiOrio, J. M. Freeman, S. Janzou, A. Dobos, D. Ryberg, *SAM Photovoltaic Model Technical Reference 2016 Update*, National Renewable Energy Lab. (NREL), Golden, CO **2018**.
[37] California Energy Commission, *Guidelines for California's Solar Electric Incentive Programs (Senate Bill 1)*, 4th ed. **2011**, http://ww2.arb.ca.gov/sites/default/files/barcu/regact/2013/capandtrade13/04cec.pdf.
[38] J. L. Braid, D. Riley, J. M. Pearce, L. Burnham, in *2020 47th IEEE Photovoltaic Specialists Conf. (PVSC)*, IEEE, Piscataway, NJ **2020**, pp. 1510–1516.
[39] A. P. Dobos, *PV Watts Version 5 Manual*, National Renewable Energy Lab. (NREL), Golden, CO **2014**.